catalysts

MDPI

Article

Insight into the Promoting Role of Er Modification on SO_2 Resistance for NH_3-SCR at Low Temperature over FeMn/TiO_2 Catalysts

Huan Du [1,†], Zhitao Han [1,2,*,†], Xitian Wu [1], Chenglong Li [1], Yu Gao [1], Shaolong Yang [3], Liguo Song [1,2], Jingming Dong [1,2] and Xinxiang Pan [1,2,4,*]

1 Marine Engineering College, Dalian Maritime University, Dalian 116026, China; duhuan@dlmu.edu.cn (H.D.); wuxitian@foxmail.com (X.W.); lichenglong9701@163.com (C.L.); gaoyu0924@dlmu.edu.cn (Y.G.); songliguo@dlmu.edu.cn (L.S.); dmudjm@dlmu.edu.cn (J.D.)
2 Liaoning Research Center for Marine Internal Combustion Engine Energy-Saving, Marine Engineering College, Dalian Maritime University, Dalian 116026, China
3 School of Naval Architecture and Ocean Engineering, Huazhong University of Science and Technology, Wuhan 430074, China; yangsl@hust.edu.cn
4 School of Electronic and Information Technology, Guangdong Ocean University, Zhanjiang 524088, China
* Correspondence: hanzt@dlmu.edu.cn (Z.H.); panxx@dlmu.edu.cn (X.P.); Tel.: +86-411-8472-3321 (Z.H. & X.P.)
† These authors contributed equally to this work and should be considered co-first authors.

Abstract: Er-modified FeMn/TiO_2 catalysts were prepared through the wet impregnation method, and their NH_3-SCR activities were tested. The results showed that Er modification could obviously promote SO_2 resistance of FeMn/TiO_2 catalysts at a low temperature. The promoting effect and mechanism were explored in detail using various techniques, such as BET, XRD, H_2-TPR, XPS, TG, and in-situ DRIFTS. The characterization results indicated that Er modification on FeMn/TiO_2 catalysts could increase the Mn^{4+} concentration and surface chemisorbed labile oxygen ratio, which was favorable for NO oxidation to NO_2, further accelerating low-temperature SCR activity through the "fast SCR" reaction. As fast SCR reaction could accelerate the consumption of adsorbed NH_3 species, it would benefit to restrain the competitive adsorption of SO_2 and limit the reaction between adsorbed SO_2 and NH_3 species. XPS results indicated that ammonium sulfates and Mn sulfates formed were found on Er-modified FeMn/TiO_2 catalyst surface seemed much less than those on FeMn/TiO_2 catalyst surface, suggested that Er modification was helpful for reducing the generation or deposition of sulfate salts on the catalyst surface. According to in-situ DRIFTS the results of, the presence of SO_2 in feeding gas imposed a stronger impact on the NO adsorption than NH_3 adsorption on Lewis acid sites of Er-modified FeMn/TiO_2 catalysts, gradually making NH_3-SCR reaction to proceed in E–R mechanism rather than L–H mechanism.

Keywords: FeMn/TiO_2; Er modification; SCR; SO_2 resistance; low temperature

Citation: Du, H.; Han, Z.; Wu, X.; Li, C.; Gao, Y.; Yang, S.; Song, L.; Dong, J.; Pan, X. Insight into the Promoting Role of Er Modification on SO_2 Resistance for NH_3-SCR at Low Temperature over FeMn/TiO_2 Catalysts. *Catalysts* **2021**, *11*, 618. https://doi.org/10.3390/catal11050618

Academic Editor: Feng Gao

Received: 13 April 2021
Accepted: 10 May 2021
Published: 11 May 2021

1. Introduction

Nitrogen oxides (NO_x) emitted from diesel engines and industrial processes are significant atmospheric pollutants, which can lead to a number of environmental problems, such as acid rain, photochemical smog, ozone depletion, and greenhouse effects [1–4]. During the past decades, a number of NO_x removal technologies have been developed with the purpose of abating NO_x emissions. Among them, selective catalytic reduction (SCR) with NH_3 (or urea) as a reductant is an effective and economic NO_x removal technique. It has been widely used in stationary and mobile sources [5–7]. In SCR systems, catalysts play a critical role in creating an efficient reaction and controlling the construction cost [8]. At present, V_2O_5-WO_3/TiO_2 and V_2O_5-MoO_3/TiO_2 catalysts have been used extensively in commercial projects. However, there are still several disadvantages, such as the narrow catalytic temperature window (300–400 °C) and toxic effect of vanadium species, limiting their further applications [9,10]. Therefore, it is of great significance to develop vanadium-free SCR catalysts with excellent catalytic activities at low temperatures (<250 °C).

In recent years, more and more researchers around the world are trying to develop high-activity low-temperature SCR catalysts. Several kinds of transition metals, such as Mn, Co, Fe, Cu, and Ni, have been extensively studied and exhibited promising SCR performance [11–15]. It is worthy to point out that $FeMn/TiO_2$ catalysts have been investigated extensively due to their advantages of excellent low-temperature SCR performance, environmentally friendly nature, and low cost [16–18]. However, there are still some challenging problems for $FeMn/TiO_2$ catalysts to overcome, including poor N_2 selectivity and weak tolerance to SO_2 and H_2O.

Generally, when a certain concentration of SO_2 gas co-exists in flue gas, ammonium sulfates and/or metal sulfates are unavoidably formed on the SCR catalyst surface. They block and destroy active sites on SCR catalyst surface, causing the deactivation of low-temperature catalysts. To enhance SO_2 resistance of $FeMn/TiO_2$ catalysts, a promising method is to modify the catalysts with other metal elements, further inducing some synergetic effects between the dopants and Fe-Mn-Ti oxides [19–21]. Jiang et al. demonstrated that doping Zr in $FeMn/TiO_2$ catalyst could enhance the formation of NO_2 in the SCR reaction, thus improve the tolerance of SO_2 [19]. Hou et al. found that the addition of proper amount of praseodymium (Pr) to $FeMn/TiO_2$ catalyst could restrain the deposition of ammonium sulfates, thus improve the catalyst stability against SO_2 poisoning [22]. A similar conclusion was drawn from their other work in whichSO_2 resistance for NH_3-SCR at low temperature was enhanced by the doping of lanthanum (La) [23]. The adsorption and oxidation of SO_2 on the catalyst were inhibited by La modification.

Erbium (Er) is a kind of rare earth element. It has been applied as a doping additive in various fields due to the incompletely occupied 4f and empty 5d orbitals [24]. For example, Er-doped ZnO (EZO) have been widely studied and expected as one of the promising materials for ZnO based optoelectronic device. The incorporation of Er could affect the band gap and optical constants of ZnO thin films [25]. Er was also used to enhance the sonocatalytic performance of organic dye degradation [26]. The prepared Er^{3+}:$YAlO_3/TiO_2$-Fe_2O_3 composite demonstrated a good sonocatalytic activity. Er^{3+} ion is an attractive optical activator and displays the richest spectra in the UV-vis-IR range due to its rich energy level structure.

The application of Er in the field of NH_3-SCR catalysts is rare. However, it has been used as doping additives to enhance the NH_3-SCR performance of V and Ce based catalysts. Vargas et al. found that Er modification on V_2O_5-WO_3/TiO_2 catalyst could improve the catalytic activity of catalysts after ageing [27], and the addition of Er caused modifications in symmetric deformation modes of ammonia coordinated on Lewis acid sites. Casanova et al. found that Er mixed with $FeVO_x$ supported on TiO_2-WO_3-SiO_2 could enhance the structural and textural stability of the system by hindering the transformation of anatase to rutile, thus enhance activity after thermal treatment [28]. Kim et al. found that Er doping in $CeVO_x$ catalyst could enhance redox features and improve the quantities of acid sites and defects. This led to the high-performance of NH_3-SCR reaction [29]. Jin et al. found that Er doping could increase oxygen storage capacities and oxygen vacancy concentrations of $CeZr/TiO_2$ catalysts, resulting in excellent SCR activity and SO_2 resistance [30]. It was considered that the introduction of Er into SCR catalysts was in favor of enhancing the structural and textural stability, redox property, improving the mounts of acid sites and oxygen vacancy, and blocking anatase transformation to rutile. It was possible to improve the activity and SO_2 resistance of $FeMn/TiO_2$ catalysts by doping with Er. However, to the best of our knowledge, the promotional effect of Er incorporation on SO_2 resistance for NH_3-SCR at low temperature over $FeMn/TiO_2$ catalysts has not been investigated yet.

In the present study, a series of Er-modified $FeMn/TiO_2$ catalysts with different Er/Mn molar ratios were successfully synthesized via the wet impregnating method. NH_3-SCR activity and SO_2 resistance over the prepared catalysts were tested. The promotional effects of Er modification on SO_2 resistance were studied systematically by various characterization techniques with the fresh and used catalysts. Finally, the possible mechanisms for the excellent SO_2 tolerance over Er-modified FeMn/TiO_2 catalysts were discussed.

2. Results

2.1. Low Temperature SCR Activity and SO_2 Resistance

Figure 1a and Figure S1a show the activities of Er_xFeMn/TiO_2 catalysts prepared with different Er/Mn molar ratios across a temperature window of 60–240 °C. Compared to the FeMn/TiO_2 catalyst, $Er_{0.01}$FeMn/TiO_2 and $Er_{0.05}$FeMn/TiO_2 catalysts exhibited higher NO_x conversion efficiencies over the whole temperature range. But the activity at low temperature (<120 °C) decreased sharply when further increasing Er doping amount. The result indicated that, the low-temperature catalytic performance of FeMn/TiO_2 catalyst could be enhanced by doping only a small amount of Er. As shown in Figure 1a, $Er_{0.05}$FeMn/TiO_2 catalyst possessed more than 95% NO_x conversion efficiency in the temperature range of 120–240 °C. Since the NO_x conversion performance of $Er_{0.05}$FeMn/TiO_2 catalyst was better than those of other catalysts over the whole temperature range, a proper Er doping molar ratio of 0.05 (Er/Mn) was chose for further investigation in this work.

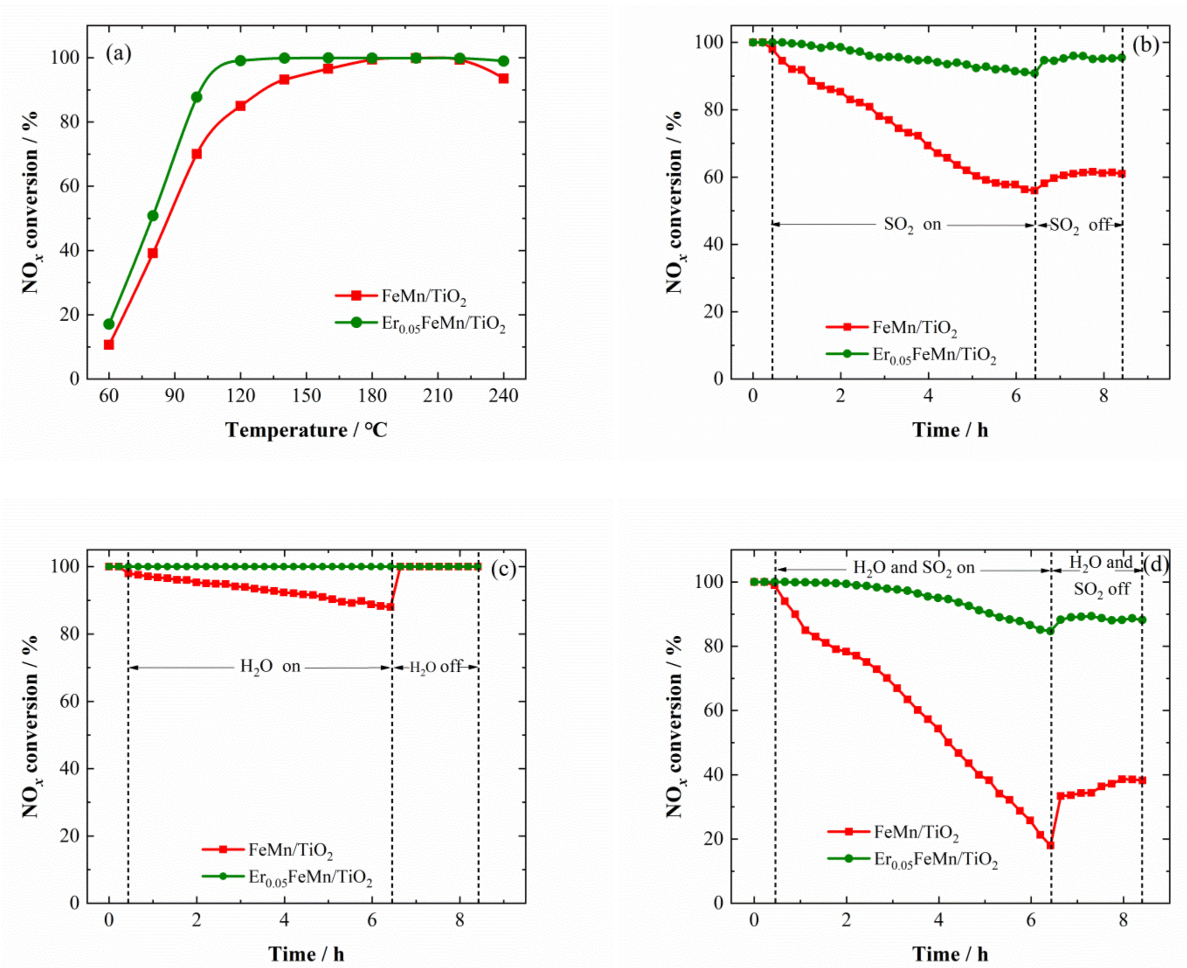

Figure 1. NO_x conversion (**a**), resistance to sulfur poisoning test (**b**), resistance to water vapor poisoning test (**c**), resistance to water vapor and sulfur poisoning test (**d**) during the NH_3-SCR reaction over FeMn/TiO_2 and $Er_{0.05}$FeMn/TiO_2 catalysts. (Reaction conditions: 1 mL catalyst, [NO] = [NH_3] = 500 ppm, [O_2] = 5 vol.%, [SO_2] = 100 ppm (when used), 5% H_2O (when used), balanced with N_2, GSHV = 30,000 h^{-1}).

The N_2 selectivity of the prepared catalysts in the temperature range of 60–240 °C is illustrated in Figure S1b. It could be seen that the N_2 selectivity of FeMn/TiO_2 catalyst at 100 °C was 92.4%, but quickly decreased to 18.8% as reaction temperature increased to 240 °C. N_2 selectivity of the prepared FeMn/TiO_2 catalyst was not so good, and this result was similar to that of some previous work [31]. The poor N_2 selectivity could be ascribed to the formation of unwanted N_2O through some side reactions [32]. When the Er doping molar ratio was 0.01, the effect of Er doping on N_2 selectivity in the whole temperature range was negligible. However, when further increasing Er doping molar ratio, N_2 selectivity of Er-modified catalysts improved obviously. The higher the Er doping molar ratio was, the better N_2 selectivity was. Here, the enhancement effect on N_2 selectivity was mainly ascribed to the inhibition of N_2O formation by the introduction of Er element.

In order to investigate the SO_2 tolerance of FeMn/TiO_2 and $Er_{0.05}$FeMn/TiO_2 catalysts, the SO_2 resistance of these two catalysts was tested in the presence of 100 ppm SO_2. As shown in Figure 1b, the NO_x conversion efficiency of FeMn/TiO_2 catalyst decreased quickly from 100% to 56.0% after introducing SO_2 in feeding gas for 6 h, and it could be restored to 61.0% after stopping SO_2 for 2 h. Compared with FeMn/TiO_2 catalyst, $Er_{0.05}$FeMn/TiO_2 catalyst displayed much better SO_2 resistance performance. After the introduction of SO_2 in feeding gas, NO_x conversion efficiency of $Er_{0.05}$FeMn/TiO_2 catalyst decreased slowly, and it could be maintained at 90.8% after exposure to 100 ppm SO_2 for 6 h. After stopping the injection of SO_2 for 2 h, NO_x conversion efficiency of $Er_{0.05}$FeMn/TiO_2 catalyst could recover to 95.5%. This result indicated that the introduction of Er element could greatly improve SO_2 resistance performance of FeMn/TiO_2 catalysts.

Generally, a small amount of H_2O vapor will exist in the flue gas of stationary and mobile sources. Here, 5% H_2O was introduced in the feeding gas to test the H_2O resistance of the selected catalysts. As shown in Figure 1c, the NO_x conversion efficiency of FeMn/TiO_2 catalyst decreased gradually from 100% to 88.0% after introducing 5% H_2O for 6 h, and it could be recovered to 100% quickly by stopping H_2O injection. This indicated that the deactivation of FeMn/TiO_2 catalyst by H_2O was reversible. By contrast, $Er_{0.05}$FeMn/TiO_2 catalyst exhibited excellent H_2O resistance performance. The introduction of 5% H_2O had little effect on the NO_x conversion efficiency of $Er_{0.05}$FeMn/TiO_2 catalyst during the whole reaction process.

The effect of coexistence of 100 ppm SO_2 and 5% H_2O in feeding gas on NO_x conversion performance of FeMn/TiO_2 catalysts with and without Er modification was also evaluated, and the results are illustrated in Figure 1d. It was clear that coexistence of SO_2 and H_2O imposed a much greater impact on FeMn/TiO_2 catalyst than that for $Er_{0.05}$FeMn/TiO_2 catalyst. NO_x conversion efficiency of FeMn/TiO_2 catalyst decreased quickly from 100% to 18.0% after introducing SO_2 and H_2O for 6 h. As to $Er_{0.05}$FeMn/TiO_2 catalyst, the change trend of NO_x conversion efficiency was similar to the case exposed to single SO_2. NO_x conversion efficiency of $Er_{0.05}$FeMn/TiO_2 catalyst decreased slowly from 100% to 84.7% after injection of SO_2 and H_2O for 6 h. Therefore, a conclusion could be drawn that the resistance to SO_2 and H_2O of FeMn/TiO_2 catalyst could be enhanced obviously by Er modification.

Previous studies reported that there were two main reasons for the deactivation of catalysts suffered from SO_2 poisoning [33–35]. On one hand, NH_3 used as NO reductant would react with SO_2 at low temperature, and the generated ammonium sulfates would cover on the catalyst surface which would block the active sites. One the other hand, the active species of the catalysts would also react with SO_2 to form inactive metal sulfates, which were destructive to the NH_3-SCR reaction. According to the SO_2 resistance tests in this work, the introduction of Er element could greatly improve SO_2 resistance performance of FeMn/TiO_2 catalysts at 200 °C. It is known that ammonium sulfates can be decomposed at 230–400 °C [36], while metal sulfates can be decomposed at a much higher temperature [37]. In view of this, it was possible that Er modification restrained the formation of ammonium sulfates and inactive metal sulfates to some extent, thus preventing the active sites being blocked or deactivated. The mechanisms of the enhancement effect of Er modification on SO_2 resistance were further analyzed through the following characterizations.

2.2. BET Results

N_2 adsorption-desorption isotherms of FeMn/TiO_2 and $Er_{0.05}$FeMn/TiO_2 catalysts are shown in Figure 2. According to IUPAC classification, the adsorption isotherms of all the catalysts were type IV, suggesting that the mesoporous structures of the prepared catalysts were not changed after SO_2 resistance tests [38]. The specific surface areas, pore volumes, and pore sizes of these catalysts were shown in Table S1. The specific surface areas of FeMn/TiO_2 and $Er_{0.05}$FeMn/TiO_2 catalysts were 58.6 and 59.5 m^2/g, respectively. After SO_2 resistance tests, the specific surface area of FeMn/TiO_2-S catalyst decreased by 10.9%, while that of $Er_{0.05}$FeMn/TiO_2-S catalyst decreased by 3.5% only. It implied that a certain amount of ammonium sulfates had been formed on the surface of both kinds of catalysts due to the reaction between NH_3 species and SO_2 [33]. As the decrease in specific surface area of $Er_{0.05}$FeMn/TiO_2 catalyst was much less than that of FeMn/TiO_2 catalyst, it demonstrated that Er modification could effectively restrain the formation of ammonium sulfates on the surface of FeMn/TiO_2 catalyst.

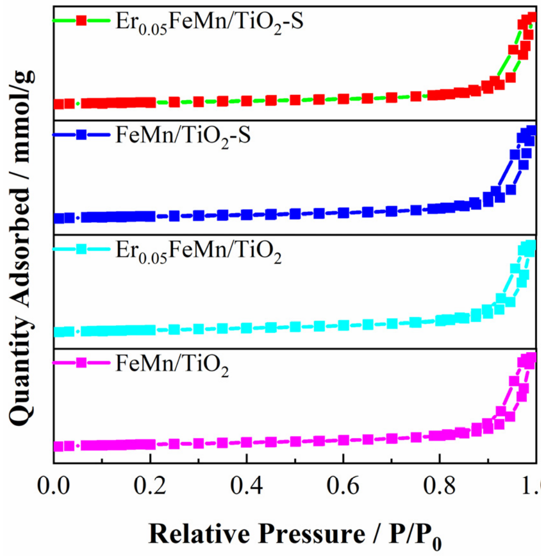

Figure 2. N_2 adsorption/desorption isotherms of the fresh and used FeMn/TiO_2 and $Er_{0.05}$FeMn/TiO_2 catalysts.

2.3. XRD Analysis

Figure 3 presents the XRD patterns of FeMn/TiO_2 and $Er_{0.05}$FeMn/TiO_2 catalysts. The diffraction peaks of 2θ at 25.3°, 36.9°, 38.6°, 48.0°, 53.9°, 55.1°, and 62.7° could be assigned to anatase TiO_2 characteristic peaks (ICCD PDF-2, 21-1272), and the diffraction peaks of 2θ at 33.0°, 38.2°, and 55.1°could be assigned to Mn_2O_3 characteristic peaks (ICCD PDF-2, 65-7467). It could be seen that all catalysts exhibited distinct anatase TiO_2 diffraction peaks, and no obvious diffraction peaks of rutile TiO_2 were found. The diffraction peaks of MnO_x in the prepared FeMn/TiO_2 catalyst matched well with the standard powder diffraction pattern of Mn_2O_3, implying Mn_2O_3 was the main crystal phase. The diffraction peaks of Mn_2O_3 in Er-modified FeMn/TiO_2 catalysts were not obvious. This suggests that Er modification promoted the transformation of MnO_x from crystalline state to highly dispersed amorphous state, which was beneficial to enhance the catalytic performance at low temperature [39,40]. After the SO_2 resistance test, there were more peaks appeared in the diffraction pattern of the used FeMn/TiO_2 catalyst, which could be ascribed to the formation of $Ti(SO_4)_2$ on catalyst surface (ICCD PDF-2, 18-1406) [41]. However, the same diffraction peak of $Ti(SO_4)_2$ was not observed in the diffraction pattern of $Er_{0.05}$FeMn/TiO_2-S catalyst. Since sulfates would cover active sites on the surface of FeMn/TiO_2 catalysts, it might be the main reason for the FeMn/TiO_2 catalyst's low SCR activity. This result also agreed well with the aforementioned SO_2 resistance test results. Furthermore, it could also demonstrate that Er doping in FeMn/TiO_2 catalysts was in favor of inhibiting the formation of sulfates on the catalyst surface, thus improving SO_2 tolerance of Er-modified $FeMn/TiO_2$ catalysts.

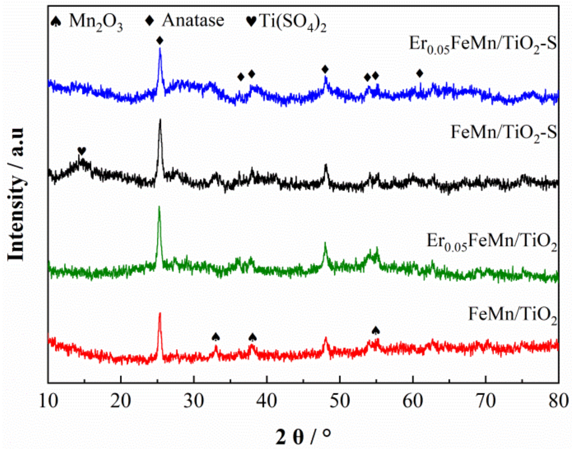

Figure 3. XRD patterns of the fresh and used $FeMn/TiO_2$ and $Er_{0.05}FeMn/TiO_2$ catalysts.

2.4. H_2-TPR Analysis

The redox properties of $FeMn/TiO_2$ and $Er_{0.05}FeMn/TiO_2$ catalysts were investigated via H_2-TPR, and the results are shown in Figure 4. The reduction peak temperatures and H_2 consumption values were listed in Table S2. As for the $FeMn/TiO_2$ catalyst, there were three reduction peaks: the low temperature reduction peak centered at 313 °C could be assigned to the reduction of MnO_2 to Mn_2O_3, the peak centered at 389 °C belonged to the reduction of Mn_2O_3 to MnO or Fe_2O_3 to Fe, and the peak centered at 582 °C belonged to the reduction of Mn_3O_4 to MnO [18,42]. Compared to $ErFeMn/TiO_2$ catalyst, all the reduction peaks of $Er_{0.05}FeMn/TiO_2$ catalyst were shifted toward low temperature direction, indicating that $Er_{0.05}FeMn/TiO_2$ catalyst had a better redox ability at low temperature. As shown in Table S2, the total H_2 consumption value of $Er_{0.05}FeMn/TiO_2$ catalyst was much more than that of $FeMn/TiO_2$ catalyst, indicating the number of reductive species on the surface of $Er_{0.05}FeMn/TiO_2$ catalyst was much more than that of $FeMn/TiO_2$ catalyst. The low reduction temperature and high H_2 consumption value demonstrated that Er modification could improve the low-temperature redox ability of $FeMn/TiO_2$ catalysts [33]. This result also agreed well with the improved SCR activity of Er-modified $FeMn/TiO_2$ catalysts at a low temperature.

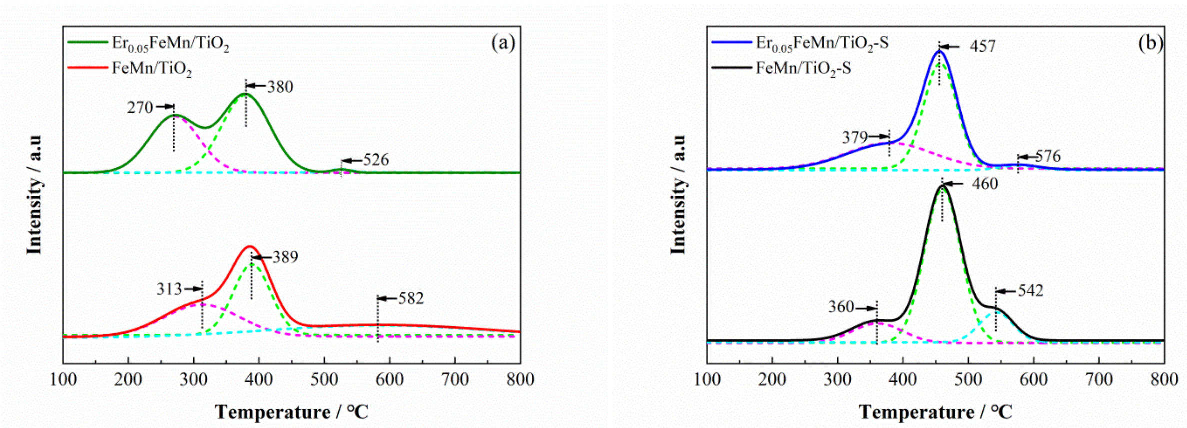

Figure 4. H_2-TPR profiles of the fresh (**a**) and used (**b**) $FeMn/TiO_2$ and $Er_{0.05}FeMn/TiO_2$ catalysts.

After SO_2 resistance tests, the reduction peaks of the used catalysts shifted toward a higher temperature zone. As shown in Figure 4b, there were three reduction peaks in the profiles of these two kinds of catalysts. Their strongest peaks were centered at 457 °C and

460 °C, respectively, which were related to the reduction of sulfate species (Mn sulfates) [33]. The corresponding H_2 consumption value (151.6 cm^3/g STP) for the strongest reduction peak of $Er_{0.05}FeMn/TiO_2$-S catalyst was less than that (194.8 cm^3/g STP) of $FeMn/TiO_2$-S catalyst. It suggested that less amount of sulfate species had been formed on the surface of $Er_{0.05}FeMn/TiO_2$ catalyst. The peaks centered at 379 and 360 °C could be assigned to the reduction of MnO_2 and Mn_2O_3 [38], and the corresponding H_2 consumption value (39.3 cm^3/g STP) for $Er_{0.05}FeMn/TiO_2$-S catalyst was much more than that (24.1 cm^3/g STP) of $FeMn/TiO_2$-S catalyst. It indicated that Er modification was favorable to maintain the redox ability of $FeMn/TiO_2$ catalyst when SO_2 coexisted in feeding gas. It was possible that Er modification on $FeMn/TiO_2$ catalyst could alleviate the deactivation due to the reaction between active species and SO_2, thus inhibiting the formation of Mn sulfate species on the catalyst surface.

2.5. XPS Analysis

The surface compositions and elementary oxidation states of the fresh and used catalysts ($FeMn/TiO_2$ and $Er_{0.05}FeMn/TiO_2$) were analyzed by X-ray photoelectron spectrometer (XPS). The spectra of Mn 2*p*, O 1*s* and S 2*p* are shown in Figure 5, and the analysis results of surface atomic concentration ratios are presented in Table S3. As shown in Figure 5a, two main peaks assigned to Mn $2p_{3/2}$ and Mn $2p_{1/2}$ were observed in the spectra of the catalysts. The overlapping peaks of Mn $2p_{3/2}$ could be divided into several sub-peaks with Shirley-type background. The obtained peaks could be ascribed to Mn^{2+} (640.9–641.7 eV), Mn^{3+} (642.0–643.0 eV) and Mn^{4+} (643.3–644.5 eV), respectively [37]. The atomic ratio of Mn^{4+} to Mn^{n+} was decided according to the peak area. As shown in Table S3, the atomic ratios of Mn^{4+}/Mn^{n+} for $FeMn/TiO_2$ and $Er_{0.05}FeMn/TiO_2$ catalysts were 31.9% and 33.9%, respectively. It suggested that more surface Mn^{4+} species were generated with the introduction of Er. This result was in accordance with the result of H_2-TPR, in which the area of the reduction peak ascribed to MnO_2 to Mn_2O_3 in the profile of $Er_{0.05}FeMn/TiO_2$ catalyst was larger than that of $FeMn/TiO_2$ catalyst. Kapteijn et al. found that NO removal efficiency at low temperature for manganese oxides decreased in an order of $MnO_2 > Mn_5O_8 > Mn_2O_3 > Mn_3O_4$ [43]. The high catalytic activity of MnO_2 (Mn^{4+}) was ascribed to its lattice defects [44]. Here, it could be inferred that the formation of more surface Mn^{4+} species was conducive for achieving a high NO_x conversion efficiency over $Er_{0.05}FeMn/TiO_2$ catalyst, as shown in Figure 1a. Compared with the fresh $FeMn/TiO_2$ and $Er_{0.05}FeMn/TiO_2$ catalysts, the peaks of Mn $2p_{3/2}$ for the used catalysts were shifted toward higher binding energy (from 641.8 and 642.1 to 642.3 and 642.5 eV, respectively). It indicated that Mn atoms in the used catalysts were not only bonded to O atoms, but also to the atoms with lower electronegativity [38]. According to S 2*p* spectra in the XPS and the analysis results of H_2-TPR, it was speculated the atoms with lower electronegativity might be originated from Mn sulfates [37,38]. The shift of binding energy of the used $FeMn/TiO_2$ catalyst before and after SO_2 resistance test was more obvious than that for $Er_{0.05}FeMn/TiO_2$ catalyst. It implied that Er modification inhibited the formation of sulfates to a certain extent. In addition, Mn atomic concentration on the surface of $FeMn/TiO_2$ catalyst decreased by 4.4% after SO_2 resistant test, while that of $Er_{0.05}FeMn/TiO_2$ catalyst decreased by only 0.5%. It demonstrated that Er modification could also inhibit the loss of Mn active species on the surface of catalysts, and thus improving the SO_2 resistance.

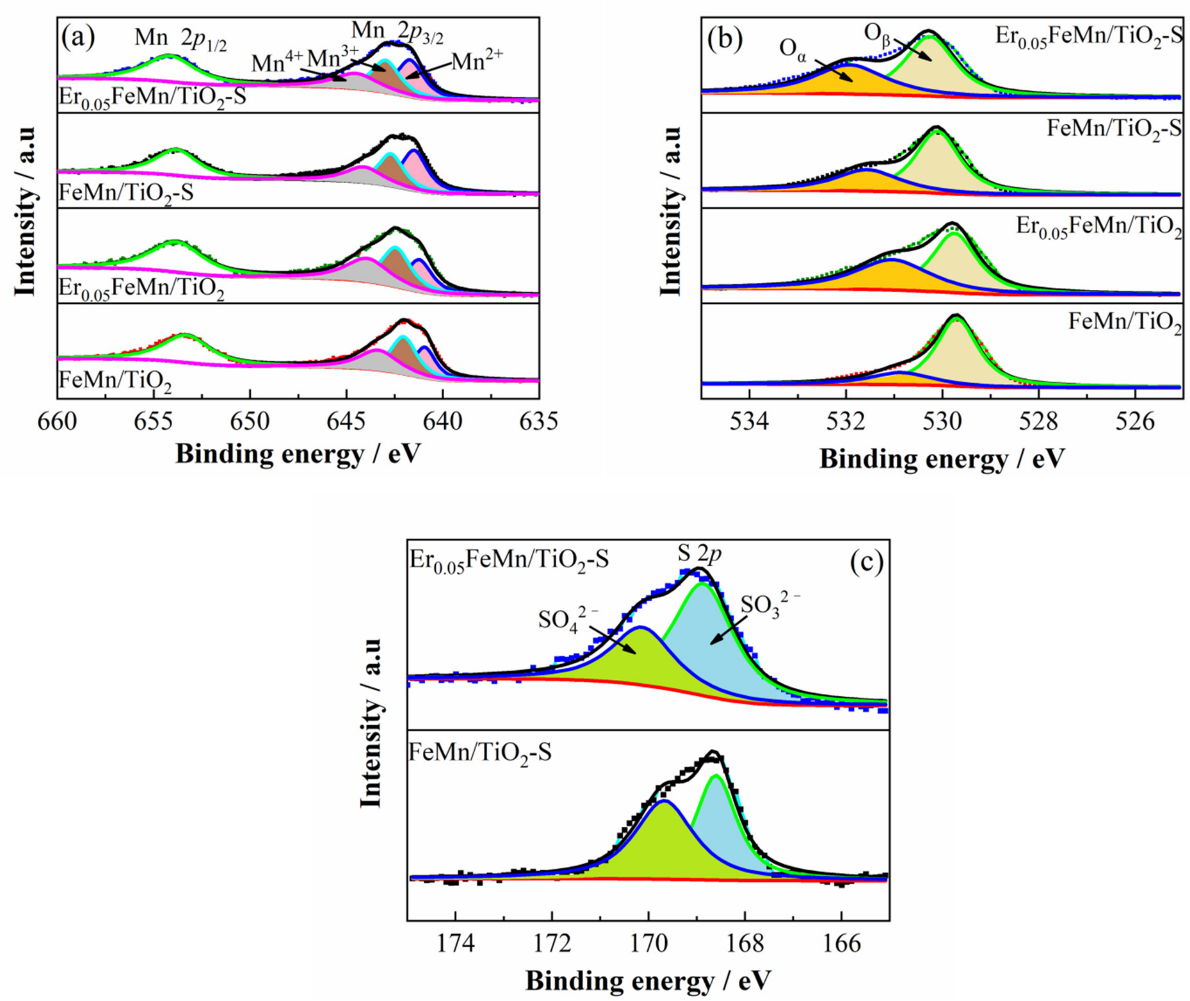

Figure 5. XPS spectra of Mn 2*p* (**a**), O 1*s* (**b**) and S 2*p* (**c**) over FeMn/TiO_2 and $Er_{0.05}$FeMn/TiO_2 catalysts.

XPS spectra of O 1*s* over the fresh and used catalysts were divided into two sub-peaks, and the results are presented in Figure 5b. The sub-peaks centered at 529.7–530.3 eV could be assigned to lattice oxygen O^{2-} (denoted as O_β). The sub-peaks centered at 530.9–531.9 eV could be assigned to surface chemisorbed labile oxygen (denoted as O_α), including defect oxide (O_2^{2-}) and hydroxyl-like group (O^-) [45,46]. The surface chemisorbed labile oxygen (O_α) was not only beneficial for oxidizing NO into NO_2, but also contributive to the generation of more active intermediate species such as –NH_2 and adsorbed NO_2 during the NH_3-SCR process [31,47]. Thus, the surface chemisorbed labile oxygen could exhibit better catalytic activity than lattice oxygen. The ratio of O_α to (O_β + O_α) was calculated according to the relative peak areas. As shown in Table S3, O_α/(O_β + O_α) ratio of $Er_{0.05}$FeMn/TiO_2 catalyst was 45.7% which was much higher than that of FeMn/TiO_2 catalyst (20.9%). It indicated that Er modification was favorable for forming more surface chemisorbed labile oxygen species on the catalyst surface. This result was in accordance with that of catalytic activity tests in which $Er_{0.05}$FeMn/TiO_2 catalyst exhibited higher NO_x conversion efficiency than that of FeMn/TiO_2 catalyst. Here the increase of chemisorbed labile oxygen ratio was ascribed to the interaction between Er and Ti, which could enhance the formation of oxygen vacancies on the catalyst surface [30]. After SO_2 resistance tests, both binding energy peaks of surface chemisorbed labile oxygen (O_α) and lattice oxygen (O_β) were shifted toward higher values compared to those of the fresh catalysts. It implied that O^- and O_2^- might be bonded with other substances when the catalysts were poisoned by SO_2. Despite that, the surface chemisorbed labile oxygen (O_α) concentration of $Er_{0.05}$FeMn/TiO_2-S catalyst was still much higher than that of the FeMn/TiO_2-S catalyst.

The XPS spectra of S 2*p* for the used catalysts are shown in Figure 5c. The two sub-peaks could be ascribed to S^{6+} in the form of SO_4^{2-} (168.6–168.9 eV) and S^{4+} in the form of SO_3^{2-} (169.7–170.1 eV), respectively [33,48,49]. It demonstrated that sulfate and sulfite salts had been formed on the catalyst surface after SO_2 resistance tests, possibly as ammonium or Mn salts. This result could not only explain the shift of binding energy found in XPS, but also confirm $Ti(SO_4)_2$ diffraction peak detected in XRD. In addition, as shown in Table S3, the contents of S and N on the surface of $Er_{0.05}FeMn/TiO_2$ catalyst were 2.8% and 1.6%, respectively, which were much less than those of $FeMn/TiO_2$ catalyst (5.3% and 2.2%), suggesting that Er modification could inhibit the formation of sulfate and/or sulfite salts on the catalyst surface when SO_2 coexisted in feeding gas.

2.6. TG Analysis

In order to further investigate the surface compounds of the catalysts poisoned by SO_2, thermogravimetric analysis of $FeMn/TiO_2$-S and $Er_{0.05}FeMn/TiO_2$-S catalysts were performed, and the TG-DTG curves are presented in Figure 6. Four temperature steps could be found in the weight loss curves of the catalysts. In the temperature range from room temperature to 200 °C (Step 1), the weight losses were assigned to the evaporation of physically absorbed H_2O on the catalysts [50]. As $(NH_4)_2SO_4$ and NH_4HSO_4 would be decomposed completely when heating temperatures were above 230 and 350 °C, respectively [51], the weight losses in the temperature range of 200 to 400 °C (Step 2) was mainly ascribed to the decomposition of $(NH_4)_2SO_4$ and NH_4HSO_4. In the temperature range of 500–650 °C (Step 3), the weight losses were related to the phase transformation of metal oxides [52]. The weight losses in the temperature range of 650–900 °C (Step 4) were mainly attributed to the decomposition of $MnSO_4$ [37]. The weight loss in the second step for $Er_{0.05}FeMn/TiO_2$-S catalyst was 0.281% which was obviously less than that for $FeMn/TiO_2$-S catalyst (0.671%). The intensities of DTG curves (Step 2) for $Er_{0.05}FeMn/TiO_2$-S catalyst were lower than those of $FeMn/TiO_2$-S catalyst. It indicated that less $(NH_4)_2SO_4$ and NH_4HSO_4 were formed on Er-modified catalyst compared with $FeMn/TiO_2$ catalyst. These results agreed well with the XPS spectra of S 2p. The TG-DTG results further proved that less sulfates formed on the surface of Er-modified $FeMn/TiO_2$ catalysts during SCR reaction in the presence of SO_2.

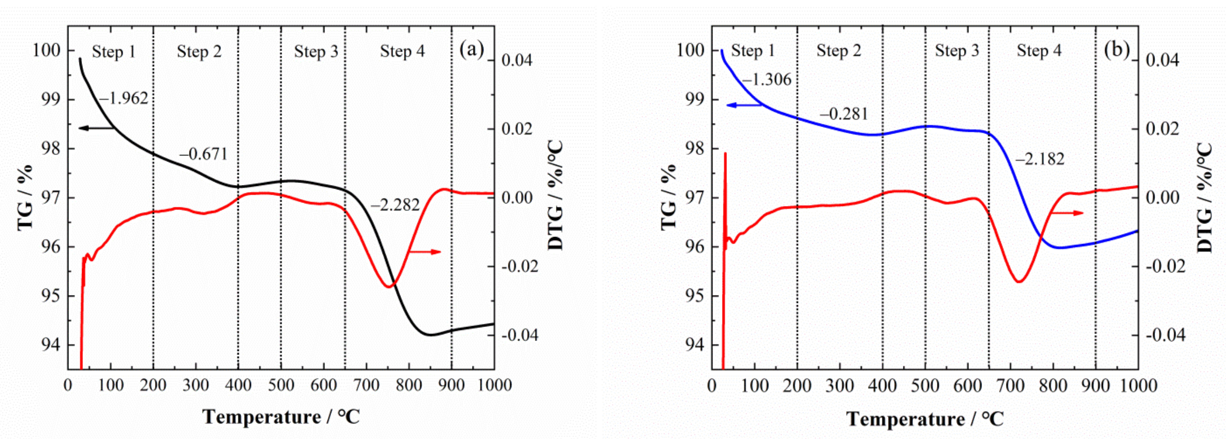

Figure 6. TGA-DTG profiles of $FeMn/TiO_2$-S (**a**) and $Er_{0.05}FeMn/TiO_2$-S (**b**) catalysts.

2.7. In-Situ DRIFTS

Aiming to get further insight into the adsorption behavior and the reaction mechanism during NH_3-SCR process in the presence of SO_2 at low temperature, in-situ DRIFTS experiments were performed at relatively low temperature (200 °C).

2.7.1. Adsorption of SO_2

Figure 7 shows in-situ DRIFTS spectra of SO_2 adsorption over $FeMn/TiO_2$ and

$Er_{0.05}FeMn/TiO_2$ catalysts. After pretreatment of each catalyst sample, 500 ppm SO_2 (50 mL/min) was introduced for 30 min, and then IR spectra were recorded. Several bands were observed in the ranges of 800–2000 cm^{-1}. The bands at 1060, 1162, 1284 cm^{-1} were ascribed to the mononuclear bidentate sulfate complex [38]. The band around 1613 cm^{-1} was attributed to the sulfates formed by the weak adsorption of SO_2, while the band at 1344 cm^{-1} was ascribed to the asymmetric stretching vibration of O=S=O in sulfates [38]. It could be seen that the intensities of all the bands over $Er_{0.05}FeMn/TiO_2$ catalyst were similar with those over $FeMn/TiO_2$ catalyst, implying that Er modification had no obvious effect on the SO_2 adsorption over the $FeMn/TiO_2$ catalyst.

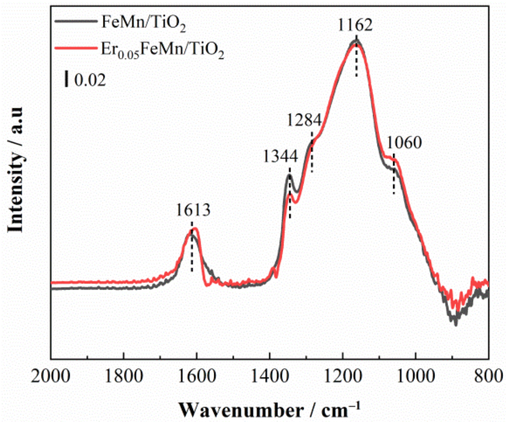

Figure 7. In-situ DRIFTS spectra of adsorption SO_2 over $FeMn/TiO_2$ and $Er_{0.05}FeMn/TiO_2$ catalysts at 200 °C.

2.7.2. Effect of SO_2 on NH_3 Adsorption on Catalyst Surface

In order to investigate the effect of SO_2 on NH_3 adsorption on the catalysts, in-situ DRIFTS spectra of the co-adsorption of NH_3 + SO_2 at 200 °C were analyzed. After pretreatment, the catalysts were pre-adsorbed with 500 ppm NH_3 (50 mL/min) for 30 min, then 100 ppm SO_2 was introduced, and the IR spectra were measured as a function of time.

As shown in Figure 8a, several bands were found in the spectra of $FeMn/TiO_2$ catalyst after the adsorption of NH_3 for 30 min. The strong absorbed bands (1166 and 1605 cm^{-1}) were assigned to coordinate NH_3 on Lewis acid sites, and the weak band (1450 cm^{-1}) was assigned to NH_4^+ species on Brønsted acid sites [37,45,53]. After the introduction of SO_2, the absorbance intensities of all the adsorbed bands increased obviously. With the introduction of SO_2, the absorbance intensity of the band (1166 cm^{-1}) assigned to NH_4^+ species on Brønsted acid sites was enhanced gradually, and a new band (1678 cm^{-1}) assigned to NH_4^+ species on Brønsted acid sites appeared in the spectra. Zhang et al. also reported that SO_2 could promote the generation of NH_4^+ species on Brønsted acid sites [38]. However, the band (1166 cm^{-1}) corresponding to NH_3 species on Lewis acid sites decreased gradually, and almost disappeared after 5 min of SO_2 injection. At the same time, three bands appeared at 1261, 1144 and 1033 cm^{-1} which were ascribed to sulfates, and they were also enhanced with the increase of SO_2 injection duration [38]. It indicated that the adsorption of NH_3 on Lewis acid sites was inhibited by the introduction of SO_2, thus reducing the SCR activity at low temperature. As shown in Figure 8b, the change in absorbed bands of $Er_{0.05}FeMn/TiO_2$ catalyst was similar to that of $FeMn/TiO_2$ catalyst. However, the intensity of the band (1169 cm^{-1}) corresponding to NH_3 species on Lewis acid sites increased gradually with the introduction of SO_2 for 30 min. According to the previous study, adsorbed NH_3 species on Lewis acid sites played a key role in SCR activity at low temperature [54]. Here it was concluded that the inhibition of competitive adsorption between SO_2 and NH_3 species on Lewis acid sites was a contributive factor to high SO_2 tolerance of Er-modified $FeMn/TiO_2$ catalysts.

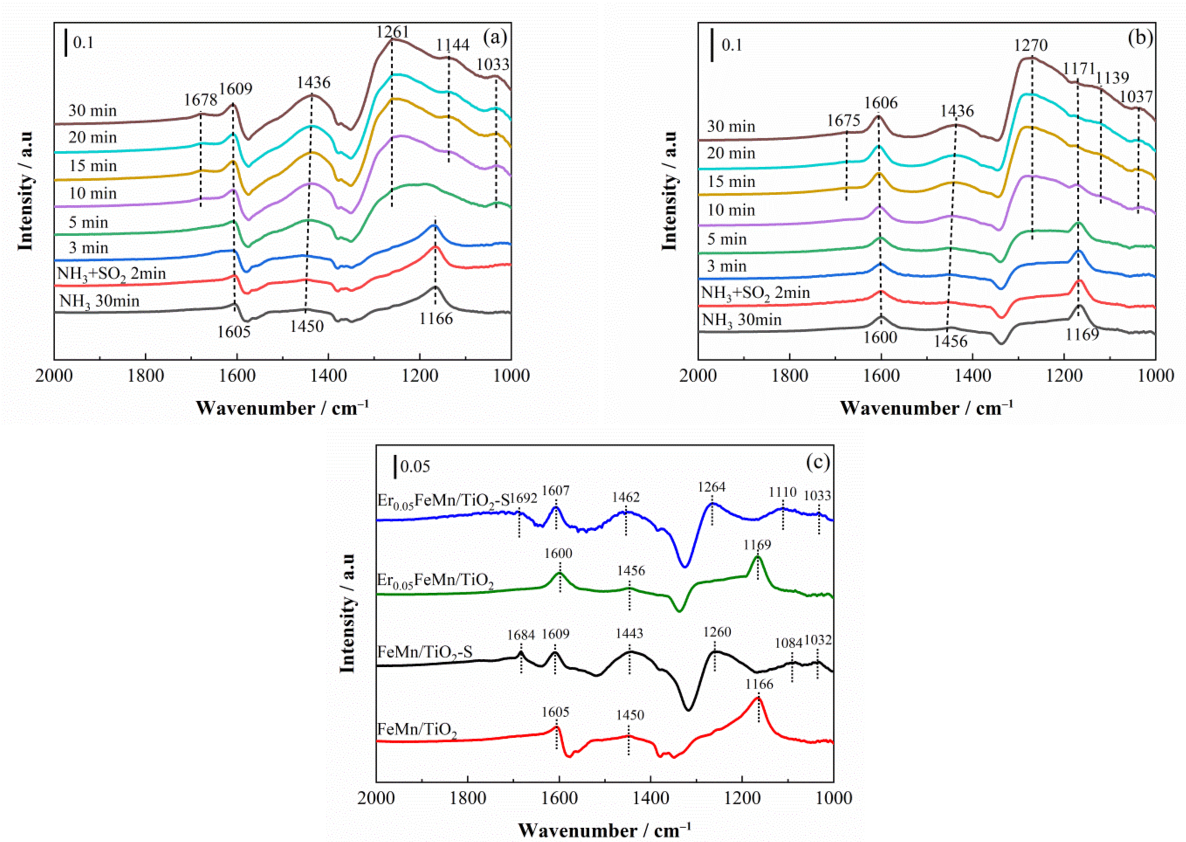

Figure 8. In-situ DRIFTS spectra FeMn/TiO_2 (**a**) and $Er_{0.05}$FeMn/TiO_2 (**b**) catalysts exposed to 500 ppm NH_3 followed by the introduction of 100 ppm SO_2 at 200 °C, and in-situ DRIFTS spectra of adsorption 500 ppm NH_3 over the fresh and used catalysts at 200 °C (**c**).

Figure 8c exhibits the in-situ DRIFTS spectra of NH_3 adsorption on FeMn/TiO_2-S and $Er_{0.05}$FeMn/TiO_2-S catalysts at 200 °C. After adsorption of 500 ppm NH_3 for 30 min and N_2 purging, several bands ascribed to various NH_3 species were found in the spectra of the fresh catalysts. The strong absorbed bands (1166 and 1605 cm^{-1}) were assigned to asymmetric and symmetric bending vibrations of the N–H bonds in NH_3 coordinated to Lewis acid sites, and the weak band (1450 cm^{-1}) was assigned to the asymmetric bending vibrations of ionic NH^{4+} bonded to the Brønsted acid sites [37,45,53,55]. The intensities of all of bands over $Er_{0.05}$FeMn/TiO_2 catalyst were higher than those over the FeMn/TiO_2 catalyst. It demonstrated that there were more Lewis acid sites and Brønsted acid sites existed on the surface of $Er_{0.05}$FeMn/TiO_2 catalyst. As to the used catalysts, the intensity of the bands (1609 and 1084 cm^{-1}) ascribed to NH_3 species adsorbed on Lewis acid sites decreased obviously due to the formation of new bands (1260 and 1032 cm^{-1}) ascribed to sulfate species [37,38]. However, the intensities of the bands (1684 and 1443 cm^{-1}) ascribed to NH^{4+} species adsorbed on Brønsted acid sites increased remarkably due to the formation of sulfate species during the SO_2 resistance tests. Some previous studies reported that the formation of sulfates on the catalyst surface could result in an increase in the amount of NH^{4+} species adsorbed on Brønsted acid sites and a decrease in the amount of NH_3 species adsorbed on Lewis acid sites [17,55,56]. Here the decrement of adsorbed NH_3 species on Lewis acid sites and the increment of adsorbed NH^{4+} species on Brønsted acid sites over $Er_{0.05}$FeMn/TiO_2-S catalyst were much less compare to FeMn/TiO_2-S catalyst. It demonstrated that Er modification improved the NH_3 adsorption on Lewis acid sites of $Er_{0.05}$FeMn/TiO_2-S catalyst, and less sulfate species formed on the surface of $Er_{0.05}$FeMn/TiO_2-S catalyst. As a result, Er modification on FeMn/TiO_2 catalyst improved the SO_2 tolerance during the NH_3-SCR process at a low temperature.

2.7.3. Effect of SO_2 on NO + O_2 Adsorption on Catalyst Surface

To understand the effect of SO_2 on NO_x adsorption on FeMn/TiO_2 and $Er_{0.05}$FeMn/TiO_2 catalysts, each catalyst was exposed to 500 ppm NO and 5% O_2 at 200 °C for 30 min, then 100 ppm SO_2 was introduced. As shown in Figure 8a, with the introduction of NO + O_2 for 30 min, several bands of adsorbed NO_x species appeared at 1575, 1380, 1366, and 1262 cm^{-1} in the spectra of FeMn/TiO_2 catalyst, which were ascribed to bidentate nitrate (1575 cm^{-1}) [53], M-NO_2 nitro compounds (1380 and 1366 cm^{-1}) [53], and monodentate nitrate (1262 cm^{-1}) [53], respectively. With the introduction of SO_2, all bands in the spectra of FeMn/TiO_2 catalyst exhibited an obvious decrease in intensity. Moreover, several new bands (1602, 1270, 1159 and 1069 cm^{-1}) ascribed to sulfates appeared with the injection of SO_2, and the absorbance intensities of these bands increased gradually. It indicated that SO_2 could restrain the adsorption of NO_x species on FeMn/TiO_2 catalysts. In other words, there was obvious competitive adsorption between NO and SO_2 which would inhibit the SCR reaction under L-H mechanism. It might be the reason for the low NO_x conversion efficiency in the presence of SO_2 for FeMn/TiO_2 catalyst [57]. The inhibiting effect of SO_2 on NO_x adsorption on $Er_{0.05}$FeMn/TiO_2 catalyst surface was quite similar to that for FeMn/TiO_2 catalyst. But the absorbance intensity of the band (1601 cm^{-1}) assigned to sulfates was obviously lower than that of FeMn/TiO_2 catalyst, indicating that less sulfate species formed on $Er_{0.05}$FeMn/TiO_2 catalyst.

Figure 9c exhibits the in-situ DRIFTS spectra of 500 ppm NO and 5% O_2 adsorption on FeMn/TiO_2 and $Er_{0.05}$FeMn/TiO_2 catalysts at 200 °C. After adsorption of NO and O_2 for 30 min and purging with N_2, several bands were found in the spectra of the fresh catalysts, which could be ascribed to bidentate nitrate (1575 cm^{-1}) [53], M-NO_2 nitro compounds (1380 and 1366 cm^{-1}) [53], and monodentate nitrate (1262 cm^{-1}) [53], respectively. After SO_2 resistance tests, the intensities of the bands ascribed to NO_x species in the spectra of both used catalysts decreased dramatically. It implied that the formation of nitrate species could be inhibited by SO_2 adsorption. In addition, the negative bands (1326 and 1311 cm^{-1}) ascribed to the displacement of the sulfates were found on FeMn/TiO_2-S and $Er_{0.05}$FeMn/TiO_2-S catalysts. This indicated that competitive adsorption between NO and SO_2 occurred on the surface of FeMn/TiO_2 and $Er_{0.05}$FeMn/TiO_2 catalysts [58].

According to the in-situ DRIFTS results mentioned above, it can be confirmed that the adsorption of NO on FeMn/TiO_2 and $Er_{0.05}$FeMn/TiO_2 catalysts was deeply inhibited by SO_2, while the inhibition effect of SO_2 on NH_3 adsorption over the $Er_{0.05}$FeMn/TiO_2 catalyst was much weaker than that over the FeMn/TiO_2 catalyst. As a result, the reaction through the Langmuir–Hinshelwood (L–H) mechanism for these two catalysts was suppressed severely. While the inhibiting effect on the reaction through Eley–Ridel (E–R) mechanisms for $Er_{0.05}$FeMn/TiO_2 catalyst was obviously weaker than that for FeMn/TiO_2 catalyst. Therefore, Er modification promoted SO_2 resistance of the FeMn/TiO_2 catalyst during the NH_3-SCR process at low temperature.

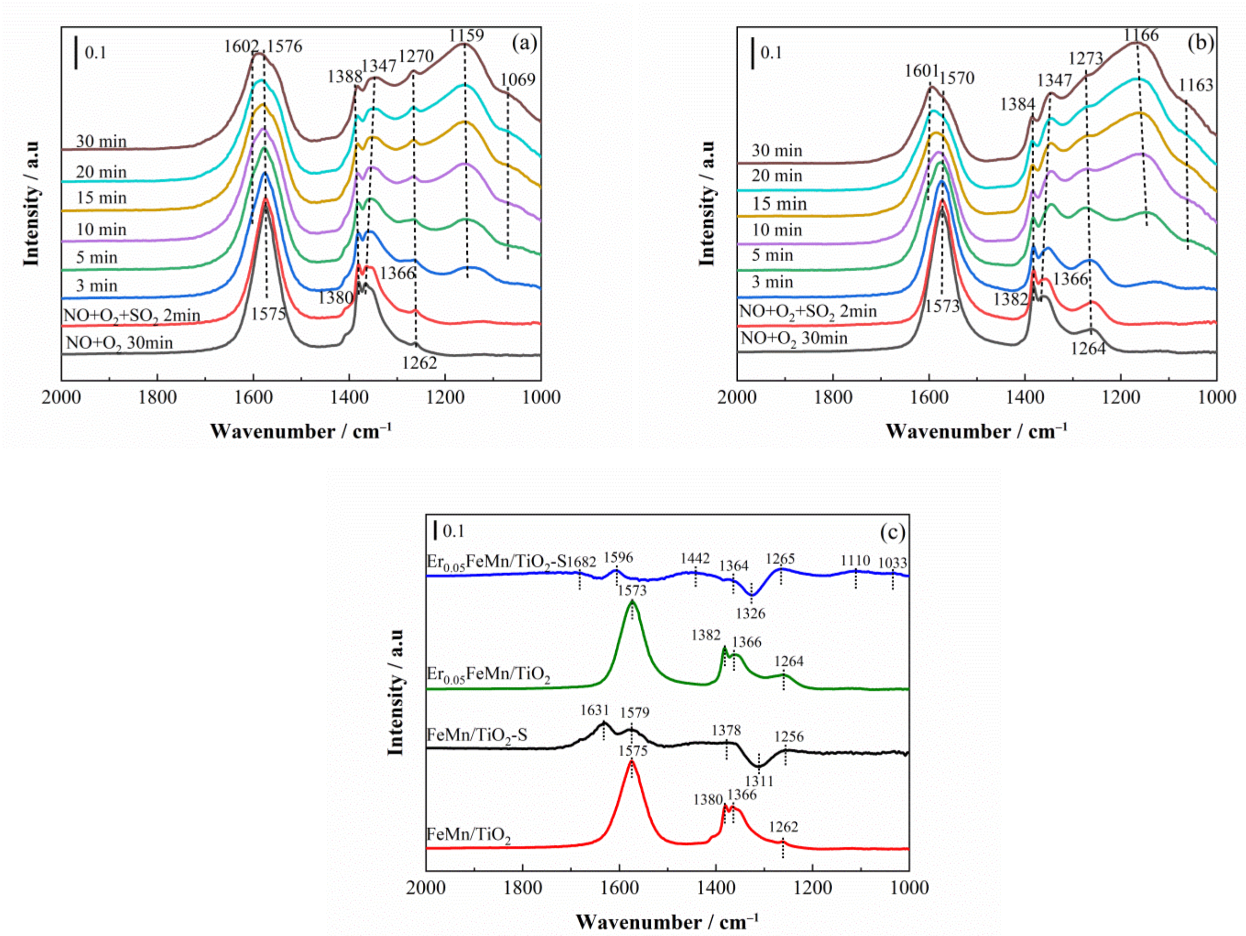

Figure 9. In-situ DRIFTS spectra FeMn/TiO$_2$ (**a**) and Er$_{0.05}$FeMn/TiO$_2$ (**b**) catalysts exposed to 500 ppm NO + 5% O$_2$ followed by the introduction of 100 ppm SO$_2$ at 200 °C, and in-situ DRIFTS spectra of adsorption 500 ppm NO + 5% O$_2$ over the fresh and used catalysts at 200 °C (**c**).

3. Discussion

In our present work, compared to the FeMn/TiO$_2$ catalyst, Er$_{0.05}$FeMn/TiO$_2$ exhibited better SCR activity and SO$_2$ tolerance at a low temperature. According to the analysis results of H$_2$-TPR, XPS and in-situ DRIFTS, the increased amounts of Mn^{4+} (Equations (5) and (6)), surface chemisorbed labile oxygen (Equation (4)) and Lewis acid sites (Equation (1)) were considered as the dominant factors which were beneficial to achieve high SCR activity at low temperature for Er$_{0.05}$FeMn/TiO$_2$ catalyst. When SO$_2$ was introduced in feeding gas, the adsorbed NH$_3$ species and Mn^{4+} active species could react with the adsorbed SO$_2$ species (Equations (10) and (11)). The generated $(NH_4)_2SO_4$ and MnSO$_4$ could not only block the active sites, but also suppress the redox cycles and the relevant reactions [59,60]. Based on the analysis results of BET, XRD, H$_2$-TPR, XPS, TG-DTG and in-situ DRIFTS, the amounts of ammonium sulfates and metal sulfates generated on Er$_{0.05}$FeMn/TiO$_2$ catalyst were obviously less than those for FeMn/TiO$_2$ catalyst. Thus, the SO$_2$ tolerance of FeMn/TiO$_2$ catalyst was remarkably enhanced by Er modification.

$$NH_3\ (g) \rightarrow NH_3\ (ad)(\text{Lewis acid sites}) \quad (1)$$

$$NO\ (g) \rightarrow NO\ (ad) \quad (2)$$

$$SO_2\ (g) \rightarrow SO_2\ (ad) \quad (3)$$

$$O_2\ (g) \rightarrow 2O^-(ad) \quad (4)$$

$$NH_3\ (ad) + Mn^{4+} + O^-(ad) \rightarrow NH_2\ (ad) + Mn^{3+} + OH \quad (5)$$

$$NO\ (ad) + Mn^{4+} + O^-(ad) \rightarrow Mn^{3+} + NO_2(ad) \quad (6)$$

$$NO\ (g)\ +\ NH_2(ad) \rightarrow NH_2\ NO(ad) \quad (7)$$

$$NH_2NO(ad) \rightarrow N_2(g) + H_2O(ad) \quad (8)$$

$$2NH_3(ad) + NO_2\ (ad) + NO(g) \rightarrow 2N_2 + 3H_2O \quad (9)$$

$$4NH_3(ad) + 2SO_2(ad) + O_2 + 2H_2O \rightarrow 2(NH_4)_2SO_4 \quad (10)$$

$$MnO_2 + SO_2(ad) \rightarrow MnSO_4 \quad (11)$$

$$2NH_3 + NO + NO_2 \rightarrow 2N_2 + 3H_2O \quad (12)$$

According to the result of in-situ DRIFTS, competitive adsorptions of SO_2 with NO and NH_3 would occur after the introduction of SO_2. Therefore, the adsorption and activation of NO and NH_3 on FeMn/TiO_2 catalyst would be inhibited greatly (Equations (1) and (2)), further suppressing the subsequent SCR reactions. However, coexisting SO_2 only imposed a slight impact on NH_3 adsorption on Lewis acid sites of $Er_{0.05}$FeMn/TiO_2 catalyst, thus NH_3-SCR reaction through E-R mechanism could proceed in a normal way. It played a key role for achieving excellent SO_2 tolerance over the $Er_{0.05}$FeMn/TiO_2 catalyst. In addition, XPS analysis results indicated that the amounts of Mn^{4+} and surface chemisorbed labile oxygen on the surface of $Er_{0.05}$FeMn/TiO_2 catalyst were much more than those for FeMn/TiO_2 catalyst. It was reported that abundant Mn^{4+} and surface chemisorbed labile oxygen species were beneficial for fast SCR reaction (Equation (12)) [61,62], which would accelerate the consumption of adsorbed NH_3 species on $Er_{0.05}$FeMn/TiO_2 catalyst. Therefore, the competitive adsorption of SO_2 and NH_3 species could be inhibited by Er modification on FeMn/TiO_2 catalyst. The reaction between adsorbed SO_2 and NH_3 species was limited, resulting in less ammonium sulfates formed on the surface of Er-modified FeMn/TiO_2 catalyst. According to the results and discussions mentioned above, the promotional effect and mechanism of Er modification on SO_2 resistance for NH_3-SCR at low temperature over FeMn/TiO_2 catalysts are illustrated in Figure 10.

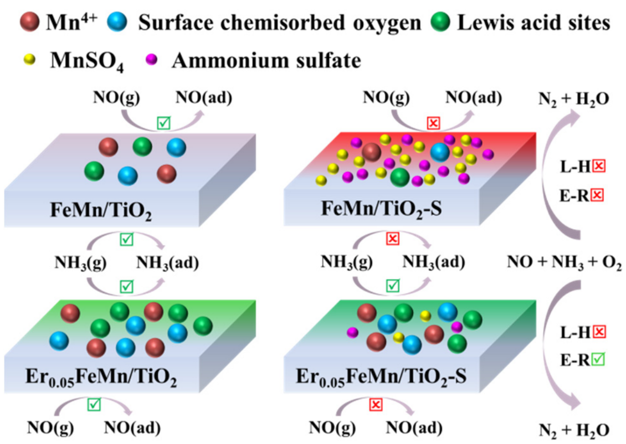

Figure 10. The promotional effect and mechanism of Er modification on SO_2 resistance for NH_3-SCR at low temperature over FeMn/TiO_2 catalysts.

4. Materials and Methods

4.1. Catalysts Preparation

A facile wet impregnating method was used to prepare Er-modified FeMn/TiO_2 catalysts. The molar ratio of Fe/Mn/Ti was fixed at 2:6:15 while Er/Mn molar ratios varied in the range of 0–0.2. In a typical preparation process, 1.686 g $Fe(NO_3)_3 \cdot 9H_2O$, 3.143 $Mn(NO_3)_2 \cdot 4H_2O$ and a certain amount of $Er(NO_3)_2 \cdot 6H_2O$ were dissolved in 100 mL deionized water, successively. 2.5 g TiO_2 powder (Degussa P25) was added into the mixture solution, followed by stirring thoroughly at 80 °C for 2 h. Then, the ammonia solution (28 wt.%) was added dropwise until solution pH reached at 10. Subsequently, the precipitate was collected by vacuum filtration, dried at 120 °C overnight, and calcined at 500 °C for 3 h in air. All the catalysts were crushed and sieved to 40–60 mesh for activity evaluation. Here Er-modified FeMn/TiO_2 catalysts were denoted as Er_xFeMn/TiO_2, where x represented various Er/Mn molar ratios (0.01, 0.05, 0.1 and 0.2). For comparison, FeMn/TiO_2 catalyst without Er modification was also prepared by using the same method without the addition of Er salt. The FeMn/TiO_2 and $Er_{0.05}$FeMn/TiO_2 catalysts after SO_2 resistance experiments were denoted as FeMn/TiO_2-S and $Er_{0.05}$FeMn/TiO_2-S, respectively.

4.2. Catalyst Activity Test

SCR activity measurements were performed using 1 mL (~0.5 g) of catalyst sample in a fixed-bed quartz reactor (i.d. 6 mm). Before each test, the catalyst was pretreated at 240 °C for 1 h in N_2 stream, and then cooled down to room temperature. Then, the catalyst was exposed to a reactant gas mixture containing 500 ppm NO, 500 ppm NH_3, 5% O_2, 5% H_2O (if used), 100 ppm SO_2 (if used), and N_2 as balance gas. The total flow rate of simulated flue gas was 500 mL/min corresponding to a gas hourly space velocity (GHSV) of 30,000 h^{-1}. After purging for 1 h, reactant gases adsorbed on catalyst surface reached an adsorption-desorption equilibrium. The reaction temperature increased from room temperature to 240 °C. The concentrations of NO, NO_2, N_2O, SO_2, NH_3, and H_2O were monitored continuously by a FTIR spectrometer (Antaris IGS, Thermo Fisher Scientific, (Waltham, MA, USA) equipped with a heated low-volume multiple-path gas cell (2 m) and a MCT detector cooled by liquid nitrogen. NO_x conversion and N_2 selectivity were calculated as follows:

$$NO_x \text{ conversion } (\%) = \frac{[NO_x]_{in} - [NO_x]_{out}}{[NO_x]_{in}} \times 100\% \tag{13}$$

$$N_2 \text{ selevtivity } (\%) = (1 - \frac{[NO_2]_{out} + 2[N_2O]_{out}}{[NO_x]_{in} - [NO_x]_{out} + [NH_3]_{in} - [NH_3]_{out}}) \times 100\% \tag{14}$$

4.3. Catalyst Characterization

The textural properties of the prepared catalysts were measured by a physisorption analyzer (ASAP 2020 PLUS, Micromeritics, Norcross, GA, USA). Before each test, the catalyst was degassed under vacuum at 350 °C for 4 h, and the N_2 adsorption-desorption data was recorded at liquid nitrogen temperature (−196 °C). The specific surface areas were calculated via the Brunauer–Emmett–Teller (BET) equation. The pore sizes and pore volumes were calculated via the Barrett–Joyner–Halenda (BJH) method.

Powder XRD patterns were carried out using an X-ray diffraction meter (Empyrean, PANalytical, Eindhoven, Noord-Brabant, The Netherlands) using Cu Kα as radiation source (λ = 0.15406 nm) at 40 kV and 30 mA. The diffractogram was recorded in a 2θ range of 10–80° with a scanning step size of 0.02°.

H_2-temperature programmed reduction (H_2-TPR) was tested using a chemisorption analyzer (Autochem II 2920, Micromeritics, Norcross, GA, USA). Prior to each test, the sample was pretreated at 350 °C for 1 h in He stream (50 mL/min), and then cooled down to 50 °C. H_2 reduction data were recorded by a TCD detector from 50 to 800 °C at a heating rate of 10 °C/min. A mixture gas of 10% H_2/Ar was used as reduction gas with a flow rate of 50 mL/min, and H_2O produced in the reduction process was removed by a cold trap.

TG analysis was performed on a thermo gravimetric analyzer (TGA-50, Shimadzu, Tokyo, Honshu, Japan). The weight loss curves of the samples were collected over a temperature range of 0–1000 °C in N_2 atmosphere with a programmed heating rate of 10 °C/min.

X-ray photoelectron spectroscopy (XPS) profiles were collected using a surface analysis photoelectron spectrometer (AXIS-ULTRA DLD-600W, Shimadzu, Tokyo, Honshu, Japan), with Al Kα as radiation source at 300 W. All binding energies were standardized to the adventitious C 1*s* peak at 284.8 eV. The pass energies of survey spectrum and high-resolution spectrum were 100 and 30 eV, respectively. Line shapes with sum of Gaussian and Lorentzian functions and Shirley-type background were applied for fitting XPS spectra.

In-situ DRIFTS measurements were performed on an FTIR spectrometer (Nicolet iS50, Thermo Fisher Scientific, Waltham, MA, USA) equipped with a MCT/A detector cooled by liquid nitrogen and a high-temperature reaction chamber (Praying Mantis, Harrick, Waltham, MA, USA). Prior to each test, the catalyst was pretreated in a N_2 flow at 200 °C for 30 min. Then, the background spectra recorded in N_2 flow were automatically subtracted from the corresponding spectra. All DRIFTS spectra were collected by accumulating 64 scans with a resolution of 4 cm^{-1} as a function of time.

5. Conclusions

In this work, the effect and mechanism of Er modification on SO_2 resistance over FeMn/TiO_2 catalysts were investigated systematically. The results showed that Er modification on FeMn/TiO_2 catalysts could effectively improve SO_2 tolerance at low temperature. After exposure to 100 ppm SO_2 for 6 h, $Er_{0.05}$FeMn/TiO_2 catalyst still exhibited more than 90% NO_x conversion efficiency at 200 °C. BET results indicated that Er doping could alleviate the decrease of specific surface area of FeMn/TiO_2 catalyst in the presence of SO_2. Less sulfates were confirmed on $Er_{0.05}$FeMn/TiO_2-S catalyst compared with those for FeMn/TiO_2-S catalyst. The XPS results indicated that Er modification could result in an increase in the concentrations of surface Mn^{4+} species and chemisorbed liable oxygen on both fresh and used catalyst. In-situ DRIFTS spectra revealed that Er modification could effectively alleviate the inhibiting effect of coexisting SO_2 on NH_3 adsorption. NH_3-SCR reaction for Er-modified FeMn/TiO_2 catalysts could proceed through E-R mechanism in almost a normal way rather than L-H mechanism. As a result, superior NO_x conversion performance could be achieved on Er-modified FeMn/TiO_2 catalyst, even in the presence of SO_2.

Supplementary Materials: The following are available online at https://www.mdpi.com/article/10.3390/catal11050618/s1, Figure S1: (a) NO_x conversion, (b) N_2 selectivity in the NH_3-SCR reaction (Reaction conditions: 1 mL catalyst, [NO] = [NH_3] = 500 ppm, [O_2] = 5 vol.%, [H_2O] = 5 vol.% (when used), [SO_2] = 100 ppm (when used), balanced with N_2, GSHV = 30,000 h^{-1}). Figure S2: EDS mapping of FeMn/TiO_2 and $Er_{0.05}$FeMn/TiO_2 catalysts. Figure S3: XPS survey spectrum of $Er_{0.05}$FeMn/TiO_2 catalyst. Table S1: Textural properties of the fresh and used catalysts. Table S2: H_2-TPR results of the fresh and used catalysts. Table S3: Calculation results of surface atomic concentration ratios of Fe, Mn and O in the fresh and used catalysts. Table S4: Surface element contents of FeMn/TiO_2 and $Er_{0.05}$FeMn/TiO_2 catalysts.

Author Contributions: Conceptualization, Z.H.; validation, Z.H.; supervision, Z.H.; investigation, Z.H. and H.D.; formal analysis, X.W., C.L. and Y.G.; methodology, J.D. and L.S.; data curation, S.Y.; funding acquisition, Z.H., J.D., L.S., S.Y. and X.P.; writing—original draft, H.D.; writing—review & editing, Z.H.; project administration, Z.H. and X.P. All authors have read and agreed to the published version of the manuscript.

Funding: This research was funded by National Natural Science Foundation of China (51779024, 51809100, 52071046, 51979022, 51979045), Natural Science Foundation of Liaoning Province of China (2020MS130), National Key Research and Development Program of China (2017YFC1404600), and Fundamental Research Funds for the Central Universities (3132019330).

Data Availability Statement: The study did not report any extra data.

Conflicts of Interest: The authors declare no conflict of interest. The funders had no role in the design of the study; in the collection, analyses, or interpretation of data; in the writing of the manuscript, or in the decision to publish the results.

References

1. Su, Z.H.; Ren, S.; Chen, Z.C.; Yang, J.; Zhou, Y.H.; Jiang, L.J.; Yang, C. Deactivation effect of CaO on Mn-Ce/AC catalyst for SCR of NO with NH_3 at low temperature. *Catalysts* **2020**, *10*, 873. [CrossRef]
2. Zhu, N.; Shan, W.P.; Lian, Z.H.; Zhang, Y.; Liu, K.; He, H. A superior Fe-V-Ti catalyst with high activity and SO_2 resistance for the selective catalytic reduction of NO_x with NH_3. *J. Hazard. Mater.* **2020**, *382*, 120970. [CrossRef]
3. Zhu, J.; Liu, Z.D.; Xu, L.; Ohnishi, T.; Yanaba, Y.; Ogura, M.; Wakihara, T.; Okubo, T. Understanding the high hydrothermal stability and NH_3-SCR activity of the fast-synthesized ERI zeolite. *J. Catal.* **2020**, *391*, 346–356. [CrossRef]
4. Zhou, G.Y.; Maitarad, P.; Wang, P.L.; Han, L.P.; Yan, T.T.; Li, H.R.; Zhang, J.P.; Shi, L.Y.; Zhang, D.S. Alkali-resistant NO_x reduction over SCR catalysts via boosting NH_3 adsorption rates by in situ constructing the sacrificed sites. *Environ. Sci. Technol.* **2020**, *54*, 13314–13321. [CrossRef]
5. Ye, D.; Wang, X.X.; Liu, H.; Wang, H.N. Insights into the effects of sulfate species on CuO/TiO_2 catalysts for NH_3-SCR reactions. *Mol. Catal.* **2020**, *496*, 111191. [CrossRef]
6. Zhao, X.Y.; Ma, S.B.; Li, Z.B.; Yuan, F.L.; Niu, X.Y.; Zhu, Y.J. Synthesis of Ce_nTiO_x flakes with hierarchical structure and its enhanced activity for selective catalytic reduction of NO_x with NH_3. *Chem. Eng. J.* **2020**, *392*, 123801. [CrossRef]
7. Zhang, N.Q.; Li, L.C.; Guo, Y.Z.; He, J.D.; Wu, R.; Song, L.Y.; Zhang, G.Z.; Zhao, J.S.; Wang, D.S.; He, H. A MnO_2-based catalyst with H_2O resistance for NH_3-SCR: Study of catalytic activity and reactants-H_2O competitive adsorption. *Appl. Catal. B Environ.* **2020**, *270*, 118860. [CrossRef]
8. Fan, Y.M.; Ling, W.; Huang, B.C.; Dong, L.F.; Yu, C.L.; Xi, H.X. The synergistic effects of cerium presence in the framework and the surface resistance to SO_2 and H_2O in NH_3-SCR. *J. Ind. Eng. Chem.* **2017**, *56*, 108–119. [CrossRef]
9. Ye, L.M.; Lu, P.; Chen, X.B.; Fang, P.; Peng, Y.; Li, J.H.; Huang, H.B. The deactivation mechanism of toluene on MnO_x-CeO_2 SCR catalyst. *Appl. Catal. B Environ.* **2020**, *277*, 119257. [CrossRef]
10. Yan, T.; Liu, Q.; Wang, S.H.; Xu, G.; Wu, M.H.; Chen, J.J.; Li, J.H. Promoter rather than inhibitor: Phosphorus incorporation accelerates the activity of V_2O_5-WO_3/TiO_2 catalyst for selective catalytic reduction of NO_x by NH_3. *ACS Catal.* **2020**, *10*, 2747–2753. [CrossRef]
11. Yan, R.; Lin, S.X.; Li, Y.L.; Liu, W.M.; Mi, Y.Y.; Tang, C.J.; Wang, L.; Wu, P.; Peng, H.G. Novel shielding and synergy effects of Mn-Ce oxides confined in mesoporous zeolite for low temperature selective catalytic reduction of NO_x with enhanced SO_2/H_2O tolerance. *J. Hazard. Mater.* **2020**, *396*, 122592. [CrossRef]
12. Wang, Z.Y.; Guo, R.T.; Shi, X.; Liu, X.Y.; Qin, H.; Liu, Y.Z.; Duan, C.P.; Guo, D.Y.; Pan, W.G. The superior performance of $CoMnO_x$ catalyst with ball-flowerlike structure for low-temperature selective catalytic reduction of NO_x by NH_3. *Chem. Eng. J.* **2020**, *381*, 122753. [CrossRef]
13. Lyu, Z.K.; Niu, S.L.; Lu, C.M.; Zhao, G.J.; Gong, Z.Q.; Zhu, Y. A density functional theory study on the selective catalytic reduction of NO by NH_3 reactivity of α-Fe_2O_3 (001) catalyst doped by Mn, Ti, Cr and Ni. *Fuel* **2020**, *267*, 117147. [CrossRef]
14. Li, R.; Wang, P.Q.; Ma, S.B.; Yuan, F.L.; Li, Z.B.; Zhu, Y.J. Excellent selective catalytic reduction of NO_x by NH_3 over Cu/SAPO-34 with hierarchical pore structure. *Chem. Eng. J.* **2020**, *379*, 122376. [CrossRef]
15. Zhao, J.J.; Yu, Y.B.; Han, X.; He, H. Fuel reforming over Ni-based catalysts coupled with selective catalytic reduction of NO_x. *Chin. J. Catal.* **2013**, *34*, 1407–1417. [CrossRef]
16. Du, H.; Han, Z.T.; Wang, Q.M.; Gao, Y.; Gao, C.; Dong, J.M.; Pan, X.X. Effects of ferric and manganese precursors on catalytic activity of Fe-Mn/TiO_2 catalysts for selective reduction of NO with ammonia at low temperature. *Environ. Sci. Pollut. Res.* **2020**, *27*, 40870–40881. [CrossRef] [PubMed]
17. Jiang, B.Q.; Wu, Z.B.; Liu, Y.; Lee, S.C.; Ho, W.K. DRIFT study of the SO_2 effect on low-temperature SCR reaction over Fe-Mn/TiO_2. *J. Phys. Chem. C* **2010**, *114*, 4961–4965. [CrossRef]
18. Putluru, S.S.R.; Schill, L.; Jensen, A.D.; Siret, B.; Tabaries, F.; Fehrmann, R. Mn/TiO_2 and Mn-Fe/TiO_2 catalysts synthesized by deposition precipitation-promising for selective catalytic reduction of NO with NH_3 at low temperatures. *Appl. Catal. B Environ.* **2015**, *165*, 628–635. [CrossRef]
19. Jiang, B.Q.; Deng, B.Y.; Zhang, Z.Q.; Wu, Z.B.; Tang, X.J.; Yao, S.L.; Lu, H. Effect of Zr addition on the low-temperature SCR activity and SO_2 tolerance of Fe-Mn/Ti catalysts. *J. Phys. Chem. C* **2012**, *118*, 14866–14875. [CrossRef]
20. Choi, H.; Jeong, Y.E.; Kumar, P.A.; Lee, K.Y.; Ha, H.P. Sb modified Fe-Mn/TiO_2 catalyst for the reduction of NO_x with NH_3 at low temperatures. *Res. Chem. Intermed.* **2018**, *44*, 3737–3751. [CrossRef]
21. Zhu, Y.W.; Zhang, Y.P.; Xiao, R.; Huang, T.J.; Shen, K. Novel holmium-modified Fe-Mn/TiO_2 catalysts with a broad temperature window and high sulfur dioxide tolerance for low-temperature SCR. *Catal. Commun.* **2017**, *88*, 64–67. [CrossRef]
22. Hou, X.X.; Chen, H.P.; Liang, Y.H.; Yang, X.; Wei, Y.L. Pr-doped modified Fe-Mn/TiO_2 catalysts with a high activity and SO_2 tolerance for NH_3-SCR at low-temperature. *Catal. Lett.* **2020**, *150*, 1041–1048. [CrossRef]
23. Hou, X.X.; Chen, H.P.; Liang, Y.H.; Wei, Y.L.; Li, Z.Q. La modified Fe-Mn/TiO_2 catalysts to improve SO_2 resistance for NH_3-SCR at low-temperature. *Catal. Surv. Asia* **2020**, *24*, 291–299. [CrossRef]
24. Yang, P.; Lu, C.; Hua, N.P.; Du, Y.K. Titanium dioxide nanoparticles Co-doped with Fe^{3+} and Eu^{3+} ions for photocatalysis. *Mater. Lett.* **2002**, *57*, 794–801. [CrossRef]
25. Mao, C.Y.; Li, W.J.; Wu, F.; Dou, Y.Y.; Fang, L.; Ruan, H.B.; Kong, C.Y. Effect of Er doping on microstructure and optical properties of ZnO thin films prepared by sol-gel method. *J. Mater. Sci.-Mater. Electron.* **2015**, *26*, 8732–8739. [CrossRef]

26. Gao, J.Q.; Jiang, R.Z.; Wang, J.; Wang, B.X.; Li, K.; Kang, P.L.; Li, Y.; Zhang, X.D. Sonocatalytic performance of Er^{3+}:$YAlO_3/TiO_2$-Fe_2O_3 in organic dye degradation. *Chem. Eng. J.* **2011**, *168*, 1041–1048. [CrossRef]
27. Vargas, M.A.L.; Casanova, M.; Trovarelli, A.; Busca, G. An ir study of thermally stable V_2O_5-WO_3-TiO_2 SCR catalysts modified with silica and rare-earths (Ce, Tb, Er). *Appl. Catal. B Environ.* **2007**, *75*, 303–311. [CrossRef]
28. Casanova, M.; Llorca, J.; Sagar, A.; Schermanz, K.; Trovarelli, A. Mixed iron-erbium vanadate NH_3-SCR catalysts. *Catal. Today* **2015**, *241*, 159–168. [CrossRef]
29. Kim, J.; Lee, S.; Kwon, D.W.; Ha, H.P. Er composition (X)-mediated catalytic properties of $Ce_{1-x}Er_xVO_4$ surfaces for selective catalytic NO_x reduction with NH_3 at elevated temperatures. *Catal. Today* **2021**, *359*, 65–75. [CrossRef]
30. Jin, Q.J.; Shen, Y.S.; Zhu, S.M.; Li, X.H.; Hu, M. Promotional effects of Er incorporation in $CeO_2(ZrO_2)/TiO_2$ for selective catalytic reduction of NO by NH_3. *Chin. J. Catal.* **2016**, *37*, 1521–1529. [CrossRef]
31. Mu, J.C.; Li, X.Y.; Sun, W.B.; Fan, S.Y.; Wang, X.Y.; Wang, L.; Qin, M.C.; Gan, G.Q.; Yin, Z.F.; Zhang, D.K. Enhancement of low-temperature catalytic activity over a highly dispersed Fe-Mn/Ti catalyst for selective catalytic reduction of NO_x with NH_3. *Ind. Eng. Chem. Res.* **2018**, *57*, 10159–10169. [CrossRef]
32. Yang, J.; Ren, S.; Chou, Y.H.; Su, Z.H.; Yao, L.; Cao, J.; Jiang, L.J.; Hu, G.; Kong, M.; Yang, J.; et al. In situ IR comparative study on N_2O formation pathways over different valence states manganese oxides catalysts during NH_3-SCR of NO. *Chem. Eng. J.* **2020**, *397*, 125446. [CrossRef]
33. Jiang, L.J.; Liu, Q.C.; Ran, G.L.; Kong, M.; Ren, S.; Yang, J.; Li, J.L. V_2O_5-modified Mn-Ce/AC catalyst with high SO_2 tolerance for low-temperature NH_3-SCR of NO. *Chem. Eng. J.* **2019**, *370*, 810–821. [CrossRef]
34. France, L.J.; Yang, Q.; Li, W.; Chen, Z.H.; Guang, J.Y.; Guo, D.W.; Wang, L.F.; Li, X.H. Ceria modified $FeMnO_x$-enhanced performance and sulphur resistance for low-temperature SCR of NO_x. *Appl. Catal. B Environ.* **2017**, *206*, 203–215. [CrossRef]
35. Kwon, D.W.; Nam, K.B.; Hong, S.C. The role of ceria on the activity and SO_2 resistance of catalysts for the selective catalytic reduction of NO_x by NH_3. *Appl. Catal. B Environ.* **2015**, *166–167*, 37–44. [CrossRef]
36. Chang, H.Z.; Chen, X.Y.; Li, J.H.; Ma, L.; Wang, C.Z.; Liu, C.X.; Schwank, J.W.; Hao, J.M. Improvement of activity and SO_2 tolerance of Sn-modified MnO_x-CeO_2 catalysts for NH_3-SCR at low temperatures. *Environ. Sci. Technol.* **2013**, *47*, 5294–5301. [CrossRef]
37. Fan, Z.Y.; Shi, J.W.; Gao, C.; Gao, G.; Wang, B.R.; Wang, Y.; He, C.; Niu, C.M. Gd-modified MnO_x for the selective catalytic reduction of NO by NH_3: The promoting effect of Gd on the catalytic performance and sulfur resistance. *Chem. Eng. J.* **2018**, *348*, 820–830. [CrossRef]
38. Zhang, Y.P.; Li, G.B.; Wu, P.; Zhuang, K.; Shen, K.; Wang, S.; Huang, T.J. Effect of SO_2 on the low-temperature denitrification performance of Ho-modified Mn/Ti catalyst. *Chem. Eng. J.* **2019**, *400*, 122597. [CrossRef]
39. Gan, L.N.; Chen, J.J.; Peng, Y.; Yu, J.; Tran, T.; Li, K.Z.; Wang, D.; Xu, G.W.; Li, J.H. NO_x removal over V_2O_5/WO_3-TiO_2 prepared by a grinding method: Influence of the precursor on vanadium dispersion. *Ind. Eng. Chem. Res.* **2018**, *57*, 150–157. [CrossRef]
40. Chen, H.F.; Xia, Y.; Huang, H.; Gan, Y.P.; Tao, X.Y.; Liang, C.; Luo, J.M.; Fang, R.Y.; Zhang, J.; Zhang, W.K.; et al. Highly dispersed surface active species of Mn/Ce/TiW catalysts for high performance at low temperature NH_3-SCR. *Chem. Eng. J.* **2017**, *330*, 1195–1202. [CrossRef]
41. Lu, Q.; Wang, Z.X.; Guo, H.Q.; Li, K.; Zhang, Z.X.; Cui, M.S.; Yang, Y.P. Selective preparation of monocyclic aromatic hydrocarbons from ex-situ catalytic fast pyrolysis of pine over $Ti(SO_4)_2$-Mo_2N/HZSM-5 catalyst. *Fuel* **2019**, *243*, 88–96. [CrossRef]
42. Ettireddy, P.R.; Ettireddy, N.; Boningari, T.; Pardemann, R.; Smirniotis, P.G. Investigation of the selective catalytic reduction of nitric oxide with ammonia over Mn/TiO_2 catalysts through transient isotopic labeling and in situ FT-IR studies. *J. Catal.* **2012**, *292*, 53–63. [CrossRef]
43. Kapteijn, F.; Vanlangeveld, A.D.; Moulijn, J.A.; Andreini, A.; Vuurman, M.A.; Turek, A.M.; Jehng, J.M.; Wachs, I.E. Alumina-supported manganese oxide catalysts: I. Characterization: Effect of precursor and loading. *J. Catal.* **1994**, *150*, 94–104. [CrossRef]
44. Morales, M.R.; Barbero, B.P.; Cadús, L.E. Total oxidation of ethanol and propane over Mn-Cu mixed oxide catalysts. *Appl. Catal. B Environ.* **2006**, *67*, 229–236. [CrossRef]
45. Zhang, Z.P.; Li, R.M.; Wang, M.J.; Li, Y.S.; Tong, Y.M.; Yang, P.P.; Zhu, Y.J. Two steps synthesis of cetiox oxides nanotube catalyst: Enhanced activity, resistance of SO_2 and H_2O for low temperature NH_3-SCR of NO_x. *Appl. Catal. B Environ.* **2021**, *282*, 119542. [CrossRef]
46. Zhao, X.; Huang, L.; Li, H.R.; Hu, H.; Hu, X.N.; Shi, L.Y.; Zhang, D.S. Promotional effects of zirconium doped $CeVO_4$ for the low-temperature selective catalytic reduction of NO_x with NH_3. *Appl. Catal. B Environ.* **2016**, *183*, 269–281. [CrossRef]
47. Liu, Y.; Gu, T.T.; Weng, X.L.; Wang, Y.; Wu, Z.B.; Wang, H.Q. DRIFT studies on the selectivity promotion mechanism of Ca-modified Ce-Mn/TiO_2 catalysts for low-temperature NO reduction with NH_3. *J. Phys. Chem. C* **2012**, *116*, 16582–16592. [CrossRef]
48. Wang, Y.L.; Li, X.X.; Zhan, L.; Li, C.; Qiao, W.M.; Ling, L.C. Effect of SO_2 on activated carbon honeycomb supported CeO_2-MnO_x catalyst for NO removal at low temperature. *Ind. Eng. Chem. Res.* **2015**, *54*, 2274–2278. [CrossRef]
49. Romano, E.J.; Schulz, K.H. A XPS investigation of SO_2 adsorption on ceria-zirconia mixed-metal oxides. *Appl. Surf. Sci.* **2005**, *246*, 262–270. [CrossRef]
50. Sun, C.Z.; Liu, H.; Chen, W.; Chen, D.Z.; Yu, S.H.; Liu, A.N.; Dong, L.; Feng, S. Insights into the Sm/Zr co-doping effects on N_2 selectivity and SO_2 resistance of a MnO_x-TiO_2 catalyst for the NH_3-SCR reaction. *Chem. Eng. J.* **2018**, *347*, 27–40. [CrossRef]

51. Wu, Z.B.; Jin, R.B.; Wang, H.Q.; Liu, Y. Effect of ceria doping on SO_2 resistance of Mn/TiO_2 for selective catalytic reduction of NO with NH_3 at low temperature. *Catal. Commun.* **2009**, *10*, 935–939. [CrossRef]
52. Gao, L.; Li, C.T.; Li, S.H.; Zhang, W.; Du, X.Y.; Huang, L.; Zhu, Y.C.; Zhai, Y.B.; Zeng, G.M. Superior performance and resistance to SO_2 and H_2O over CoO_x-modified MnO_x/biomass activated carbons for simultaneous Hg^0 and NO removal. *Chem. Eng. J.* **2019**, *371*, 781–795. [CrossRef]
53. Wu, Z.B.; Jiang, B.Q.; Liu, Y.; Wang, H.Q.; Jin, R.B. DRIFT study of manganese/titania-based catalysts for low-temperature selective catalytic reduction of NO with NH_3. *Environ. Sci. Technol.* **2007**, *41*, 5812–5817. [CrossRef]
54. Zuo, J.L.; Chen, Z.H.; Wang, F.R.; Yu, Y.H.; Wang, L.F.; Li, X.H. Low-temperature selective catalytic reduction of NO_x with NH_3 over novel Mn-Zr mixed oxide catalysts. *Ind. Eng. Chem. Res.* **2014**, *53*, 2647–2655. [CrossRef]
55. Lian, Z.H.; Liu, F.D.; Shan, W.P.; He, H. Improvement of Nb doping on SO_2 resistance of VO_x/CeO_2 catalyst for the selective catalytic reduction of NO_x with NH_3. *J. Phys. Chem. C* **2017**, *121*, 7803–7809. [CrossRef]
56. Liu, J.; Guo, R.T.; Li, M.Y.; Sun, P.; Liu, S.M.; Pan, W.G.; Liu, S.W.; Sun, X. Enhancement of the SO_2 resistance of Mn/TiO_2 SCR catalyst by Eu modification: A mechanism study. *Fuel* **2018**, *223*, 385–393. [CrossRef]
57. Jin, R.B.; Liu, Y.; Wang, Y.; Cen, W.L.; Wu, Z.B.; Wang, H.Q.; Weng, X.L. The role of cerium in the improved SO_2 tolerance for NO reduction with NH_3 over Mn-Ce/TiO_2 catalyst at low temperature. *Appl. Catal. B Environ.* **2014**, *148–149*, 582–588. [CrossRef]
58. Han, L.P.; Cai, S.X.; Gao, M.; Hasegawa, J.; Wang, P.L.; Zhang, J.P.; Shi, L.Y.; Zhang, D.S. Selective catalytic reduction of NO_x with NH_3 by using novel catalysts: State of the art and future prospects. *Chem. Rev.* **2019**, *119*, 10916–10976. [CrossRef]
59. Tong, Y.M.; Li, Y.S.; Li, Z.B.; Wang, P.Q.; Zhang, Z.P.; Zhao, X.Y.; Yuan, F.L.; Zhu, Y.J. Influence of sm on the low temperature NH_3-SCR of NO activity and H_2O/SO_2 resistance over the $Sm_aMnNi_2Ti_7O_x$ (a = 0.1, 0.2, 0.3, 0.4) catalysts. *Appl. Catal. A-Gen.* **2020**, *590*, 117333. [CrossRef]
60. Zhang, B.L.; Liebau, M.; Suprun, W.; Liu, B.; Zhang, S.G.; Gläser, R. Suppression of N_2O formation by H_2O and SO_2 in the selective catalytic reduction of NO with NH_3 over a Mn/Ti-Si catalyst. *Catal. Sci. Technol.* **2019**, *9*, 4759–4770. [CrossRef]
61. Xiong, S.C.; Peng, Y.; Wang, D.; Huang, N.; Zhang, Q.F.; Yang, S.J.; Chen, J.J.; Li, J.H. The role of the Cu dopant on a Mn_3O_4 spinel SCR catalyst: Improvement of low-temperature activity and sulfur resistance. *Chem. Eng. J.* **2020**, *387*, 124090. [CrossRef]
62. Xie, S.Z.; Li, L.L.; Jin, L.J.; Wu, Y.H.; Liu, H.; Qin, Q.J.; Wei, X.L.; Liu, J.X.; Dong, L.H.; Li, B. Low temperature high activity of M (M = Ce, Fe, Co, Ni) doped M-Mn/TiO_2 catalysts for MH_3-SCR and in situ DRIFTS for investigating the reaction mechanism. *Appl. Surf. Sci.* **2020**, *515*, 146014. [CrossRef]